REPORT DOCUMENTATION PAGE

Form Approved
OMB No. 0704-0188

1. AGENCY USE ONLY (Leave blank)	2. REPORT DATE	3. REPORT TYPE AND DATES COVERED
	7/31/96	5/1/96 - 7/31/96

4. TITLE AND SUBTITLE
High Resolution Computerized Ionospheric Tomography Systems

5. FUNDING NUMBERS
G
N00014-95
1-0850

6. AUTHOR(S)
Helen Na

7. PERFORMING ORGANIZATION NAME(S) AND ADDRESS(ES)
University of Iowa
201 Gilmore Hall
Iowa City, IA 52242

8. PERFORMING ORGANIZATION REPORT NUMBER
HN4-96-ONRYI

9. SPONSORING/MONITORING AGENCY NAME(S) AND ADDRESS(ES)
Office of Naval Research
Ballston Tower One
800 North Quincy St.
Arlington, VA 22217-5660

10. SPONSORING/MONITORING AGENCY REPORT NUMBER

11. SUPPLEMENTARY NOTES
Attached papers published/to be published in: Proc. IES 1996, Radio Science.

12a. DISTRIBUTION/AVAILABILITY STATEMENT
Public Distribution

12b. DISTRIBUTION CODE

19960805 065

13. ABSTRACT (Maximum 200 words)

Research during the period since 5/1/96 has focused on time-frequency reconstruction and time varying imaging. The core of the space-frequency algorithm, developed in year one, has been further refined. This algorithm has been tested on more robust sets of images and cases with simulated measurement noise. The results have been extremely positive. Future work will focus on making this core algorithm into a complete CIT algorithm. The other area of research has been in the development of the time varying algorithm. The goal was to develop an algorithm that combined model based imaging with smoothness constraints to enable imaging capable of detecting motion of the ionosphere during data acquisition. Work has focused on development of the Smoothness and Conjugate Gradient Method (SCG). This algorithm uses smoothness constraints for a relaxed fit to TEC data. Work is beginning on merging this algorithm with the Residual Correction Method, developed in year one. The result will be a three-dimensional (x,y,time) time varying algorithm.

14. SUBJECT TERMS	15. NUMBER OF PAGES
Computerized Ionospheric Tomography	52
	16. PRICE CODE

17. SECURITY CLASSIFICATION OF REPORT	18. SECURITY CLASSIFICATION OF THIS PAGE	19. SECURITY CLASSIFICATION OF ABSTRACT	20. LIMITATION OF ABSTRACT
Unclassified	Unclassified	Unclassified	UL

1996 (partial year) Annual Report: High Resolution Computerized Ionospheric Tomography Systems (5/1/96 – 9/30/96)

The research funded by ONR YI Grant N00014-95-1-0850 is on the development of resolution metrics and compensation techniques for each physical parameter in the computerized ionospheric tomography (CIT) system. Research during the period since 5/1/96 has focused on time-frequency reconstruction and time varying imaging.

The core of the space-frequency algorithm was developed in year one. Since then it has been further refined and tested on more robust sets of images and cases with simulated measurement noise. The results have been extremely positive and are detailed in the revised paper by H. Na and C. Biswas, listed below. Future work will focus on making this core algorithm into a complete CIT algorithm. Key pieces of this future work will be the development of a robust interpolation routine for converting TEC data into projection slices and spectral samples on the Cartesian grid.

The other area of research has been in the development of the time varying algorithm. The goal was to develop an algorithm that combined model based imaging with smoothness constraints to enable imaging capable of detecting motion of the ionosphere during data acquisition. Work has focused on development of the Smoothness and Conjugate Gradient Method (SCG). This algorithm uses smoothness constraints for a relaxed fit to TEC data. One key in this method is the incorporation of additional measurements such as ionosonde data and DMSP data. Currently the algorithm is capable of incorporation of ionosonde data. DMSP data will be added in coming months. Work is beginning on merging this algorithm with the Residual Correction Method, developed in year one. The result will be a three-dimensional (x,y,time) time varying algorithm. Initial results of the SCG Method are detailed in the technical report by Sutton and Na, listed below.

Details of the research are presented in the attached papers.

Papers and presentations:

E. Sutton and H. Na, "Ionospheric Tomography Using Smoothness and Conjugate Gradients", Technical Report.

H. Na and C. Biswas, "A Localized Space-Frequency Algorithm for Computerized Ionospheric Tomography", Radio Science, (accepted).

E. Sutton and H. Na, "Static Tomographic Reconstruction of the Time Varying Ionosphere", Proc. of IEEE Conf. on Image Processing, 1996 (accepted).

Draft copy

Ionospheric Tomography Using Smoothness and Conjugate Gradients

Eric Sutton and Helen Na
Department of Electrical and Computer Engineering
University of Iowa, Iowa City, IA 52242

July 29, 1996

Abstract

Ionospheric tomography (IT) is a technique that is used to create images of ionospheric electron density in a vertical slice through the ionosphere. For IT the reconstruction of electron density is not uniquely determined by the data, so all IT reconstruction algorithms use a priori information. This can cause problems when the ionosphere does not behave as predicted by the model. This paper presents an ionospheric tomography algorithm that uses minimal a priori information. The tradeoff for additional flexibility is some decrease in resolution. This decrease in resolution can be partially compensated for by using additional sources of information, such as ionosonde data. An example is presented using simulated data. Using the example, the effect of including ionosonde data, using an initial guess, and calculating calibration offsets simultaneously with reconstruction is demonstrated.

1 Introduction

An ionospheric tomography (IT) system consists of a satellite and several ground stations. With this configuration, tomographic data can be collected that can then be used to reconstruct an image of ionospheric electron density in the plane defined by the ground stations and the satellite orbit [1–11]. Several experimental studies have been performed to demonstrate the feasibility of IT [12–16]. The central problem of IT is that the data generated by the IT system is incomplete, i.e. the reconstruction is not uniquely defined by the data [17–23].

Considerable effort has been expended on the part of IT researchers to design algorithms that use the incomplete IT data in the most advantageous way possible. Often the IT data and ionospheric modeling can be supplemented by other sources of data such as ionosonde data. However, many current IT reconstruction algorithms rely heavily on increasingly sophisticated a priori ionospheric models.

This reliance on ionospheric modeling leaves open the question of what happens when there is a poor match between the actual ionosphere and the ionospheric model. Therefore

there has been some recent interest in reconstruction algorithms that use more general a priori information about the ionosphere instead of a priori models. Specifically, it is known a priori that ionospheric electron density tends to be horizontally stratified, vertically smooth, and tapered to small values at low and high altitude. This information can be used to construct an algorithm that yields reasonable performance with minimal a priori information. In addition, examination of the reconstructions produced using minimal a priori information is useful in assessing the amount of information contained in the IT data itself.

Ionospheric tomography algorithms can be divided into two classes: pixel based methods and nonpixel based methods. Pixel based methods include maximum entropy reconstruction [3], model assisted ionospheric tomography [7], and reconstruction using smoothness constraints [4, 24]. Nonpixel based methods include expansion in model ionospheres [22], weighted, damped least squares [5], and residual correction method [8, 8–10].

The earliest IT algorithms used pixels as basis functions, since existing reconstruction algorithms such as algebraic reconstruction technique (ART) and multiplicative algebraic reconstruction technique (MART) can be applied. A priori information can be introduced into pixel based algorithms through an initial guess or through constraining relationships between pixel values. An initial guess often comes from an ionospheric model. Data from other sources, such as ionosonde, can be used to influence the initial guess, or can be used directly by the reconstruction algorithm.

Nonpixel basis functions have several advantages. Since ionospheric electron density is a smooth function, if the basis functions are appropriately designed smooth functions, then the ionosphere can be approximated with better accuracy using fewer basis functions than would be necessary using pixels. In addition, a priori information can be entered into the reconstruction algorithm through the choice of basis functions. The reconstruction is then constrained to lie in the image space spanned by the basis functions. The basis functions often are derived from an ionospheric model.

All of the techniques mentioned above can produce very good results in cases where there is a good match between the ionosphere and the predictions of the ionospheric model. However, the ionosphere is very dynamic, and not all the factors that influence the electron density distribution are clearly understood. If the match between the ionosphere and the model is poor, then algorithms that rely heavily on a model can produce misleading results. On the other hand, if no a priori information is used, then the quality of the reconstruction is very poor.

Ideally, IT reconstruction should involve the comparison of several reconstructions from different algorithms that use a priori information in different ways. If the a priori information is correct, then reconstructions from algorithms that use weak a priori information should be low resolution versions of reconstructions from algorithms that use a strong priori information. If there are significant differences between reconstructions that cannot be explained on the basis of reduced or enhanced resolution, then reconstructions using strong a priori information are probably not accurate.

This paper presents an algorithm that uses minimal a priori information. The new algorithm uses smoothness constraints similar to those proposed by Fehmers [24] combined with solution by the method of conjugate gradients (CG) [25]. CG was chosen over more traditional algebraic reconstruction algorithms such as ART, because the data will often be inconsistent with the smoothness constraints. The ART algorithm tends to cycle between

solutions when presented with inconsistent data [26], whereas the convergence of CG is not affected.

2 Discussion

Suppose the region of the ionosphere to be imaged is approximated by a grid of pixels, where there are I pixels in the angular direction and J pixels in the radial direction. Suppose further that there are K measurements. Then the ionospheric tomography measurements can by modeled using

$$Ax = b, \tag{1}$$

where b is a $K \times 1$ vector of measurements, x is a $IJ \times 1$ vector of image pixel values, and A is a $K \times IJ$ matrix that transforms image space into measurement space. The objective of tomographic reconstruction is to invert (1) so that the pixel values in x can be calculated from the measurements in b.

A least squares (LS) solution to (1) is a solution that minimizes

$$J(x) = \|Ax - b\|_2^2. \tag{2}$$

In general, the ionospheric tomography problem is mixed over and under determined, so that there are infinitely many solutions that minimize $J(x)$ in (2). The minimum norm least squares solution (MNLS) is the LS solution with the smallest norm, in other words, the LS solution that also minimizes $\|x\|_2^2$.

If (1) is under determined, then there are nonzero solutions to $Ax = 0$. In practical terms this means that there are nonzero distributions of ionospheric electron density that do not affect the measurements. The set of all solutions to $Ax = 0$ is the null space of (1). The null space is a sub-space of the solution space about which the measurements provide no information.

Any LS solution x_{LS} consists of two components

$$x_{LS} = x_{MN} + x_{NS}, \tag{3}$$

where x_{MN} is the MNLS solution, and x_{NS} is a solution from the null space of (1). For the MNLS solution, $x_{NS} = 0$. The MNLS solution is used for many applications, since the assumption that $x_{NS} = 0$ is the most benign assumption that can be made about the component of the solution that cannot be measured. This is not true for ionospheric tomography, because the MNLS solution will often contain many negative electron densities, and negative electron densities are clearly impossible. Therefore, for ionospheric tomography a non-zero value must be given to x_{NS} based on a priori assumptions.

For ionospheric tomography, instead of choosing the LS solution for which $\|x\|_2^2$ is minimum, it makes more sense to choose the solution that is in some sense consistent with features expected in an ionospheric electron density distribution. Suppose some matrix C can be constructed such that $\|Cx\|_2^2$ is a measure of how consistent x is with features expected in an ionospheric electron density distribution. Then if C is of full rank, there exists a unique LS solution of (1) that minimizes $\|Cx\|_2^2$.

The concept of choosing the LS solution for which $\|Cx\|_2^2$ is minimum is conceptually elegant, but does not account for some practical computational realities. The matrices A and C are both very large and sparse. Algorithms that calculate the LS solution of (1) that minimizes $\|Cx\|_2^2$ exist but do not take advantage of sparsity so are not computationally feasible for extremely large matrices. This difficulty can be circumvented by redefining $J(x)$ in (2) as

$$J(x) = \|Ax - b\|_2^2 + \alpha^2 \|Cx\|_2^2, \tag{4}$$

where α is a constant that is chosen large enough to guarantee a numerically stable unique solution but small enough that the magnitude of the error measure $J(x)$ is dominated by $\|Ax - b\|_2^2$. The minimum of $J(x)$ in (4) can be found using a sparse matrix algorithm such as conjugate gradients (CG) [25].

For ionospheric tomography it is convenient to split C into three pieces and write (4) as

$$J(x) = \|Ax - b\|_2^2 + \alpha_1^2 \|C_1 x\|_2^2 + \alpha_2^2 \|C_2 x\|_2^2 + \alpha_3^2 \|C_3 x\|_2^2, \tag{5}$$

where $\|C_1 x\|_2^2$ differentiates the image in the horizontal direction, $\|C_2 x\|_2^2$ differentiates the image twice in the vertical direction, and $\|C_3 x\|_2^2$ selects the pixels at extreme low and high altitude. These are the same three quantities suggested by Fehmers [4]. The rationale behind this is as follows: (1) The Ionosphere is known to be horizontally stratified, thus the first derivative is minimized in the horizontal direction. (2) The electron density varies over a wide range in the vertical direction but still follows a relatively smooth function, thus the second derivative is minimized to maximize smoothness in the vertical direction. (3) Electron densities become very small at extreme low and high altitude, thus the values of pixels at extreme low and high altitude are minimized.

In the following discussion of the construction of the matrices C_1, C_2, and C_3, it is assumed that when the image pixels are entered in the vector x, the image is scanned first in the horizontal direction, then in the vertical direction. The matrix C_1 takes the first derivative of the solution in the horizontal direction. The matrix C_1 is block diagonal where each $(I-1) \times I$ block is given by

$$F_1 = \begin{bmatrix} 1 & -1 & & & & \\ & 1 & -1 & & & \\ & & \ddots & \ddots & & \\ & & & 1 & -1 & \\ & & & & 1 & -1 \end{bmatrix}. \tag{6}$$

The matrix C_1 is then formed using

$$C_1 = I_J \otimes F_1, \tag{7}$$

where $\otimes$ denotes the Kronecker matrix product.

The matrix C_2 takes the second derivative of the solution in the vertical direction. The matrix C_2 is block diagonal with column reordering where each $J \times J$ block is given by

$$F_2 = \begin{bmatrix} 1 & -1 & & & & & \\ -1 & 2 & -1 & & & & \\ & -1 & 2 & -1 & & & \\ & & \ddots & \ddots & \ddots & & \\ & & & -1 & 2 & -1 & \\ & & & & -1 & 2 & -1 \\ & & & & & -1 & 1 \end{bmatrix}. \tag{8}$$

The matrix C_2 is then formed using

$$C_2 = \mathcal{Q}\,[I_I \otimes F_2], \tag{9}$$

where $\mathcal{Q}$ is an operator that reorders the columns to be consistent with the ordering of x.

The matrix C_3 selects the pixels at extreme low and high altitude, and is given by

$$C_3 = \begin{bmatrix} I_I & 0 & \cdots & 0 & 0 \\ 0 & 0 & \cdots & 0 & I_I \end{bmatrix}. \tag{10}$$

Let the matrix C be defined as

$$C = \begin{bmatrix} \alpha_1 C_1 \\ \alpha_2 C_2 \\ \alpha_3 C_3 \end{bmatrix}. \tag{11}$$

Then the matrix C is of full column rank. Consider the real valued function $u(h)$ defined for real h between 0 and 1. Assuming that the second derivative of u exists for all h, constrain u so that $u(0) = 0$, $u(1) = 0$, and $u''(h) = 0$ for all h. Then $u(h) = 0$ for all h. Similar reasoning can be used to show that C is of full column rank. Consider the vector v of length N. If v is constrained so that $v_1 = 0$, $v_N = 0$, and $F_2 v = 0$, where F_2 is as defined in (8), then $v = 0$. Repeated application of this fact shows that the only solution to $Cx = 0$ is $x = 0$, so C is of full column rank.

The the error function given by (5) corresponds to the augmented LS problem given by

$$\begin{bmatrix} A \\ C \end{bmatrix} x = \begin{bmatrix} b \\ 0 \end{bmatrix}. \tag{12}$$

Define

$$A_1 = \begin{bmatrix} A \\ C \end{bmatrix}, \tag{13}$$

and

$$b_1 = \begin{bmatrix} b \\ 0 \end{bmatrix}, \tag{14}$$

then the CG method is applied to

$$A_1^T A_1 x = A_1^T b_1. \tag{15}$$

The CG method converges if $A_1^T A_1$ is a positive definite symmetric matrix. $A_1^T A_1$ is clearly symmetric. Since C is of full column rank, A_1 also is of full column rank, so $A_1^T A_1$ is positive definite.

3 Examples

The simulated ionospheric electron density image used for the reconstructions that follow is shown in Figure 1. The original image contains two peaks centered at $\pm 15°$ latitude. The peak electron density varies from 300 to 500 km altitude. TEC data was calculated for 7 receivers placed every 10° from $-30°$ to 30°, and satellite positions every 0.25° from $-39°$ to 39°. For the reconstruction using ionosonde information, 7 ionosondes were used, one at each receiver location. The number of samples per ionosonde varies with the altitude of the peak electron density.

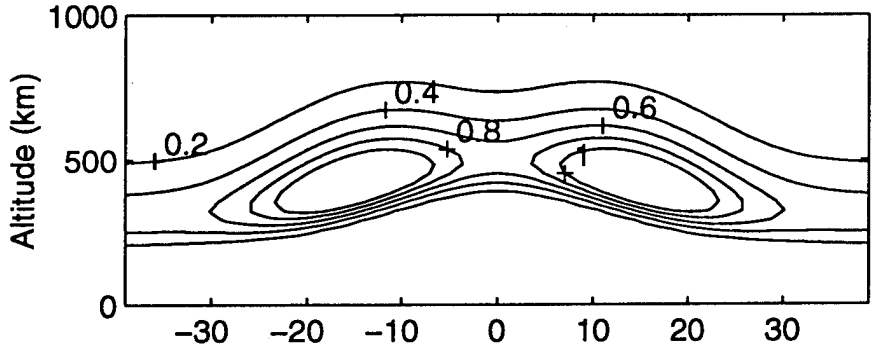

Figure 1: Original image.

For all of the reconstructions that follow, there are 128 pixels in the horizontal direction and 32 pixels in the vertical direction. A total of 500 iterations of CG are performed.

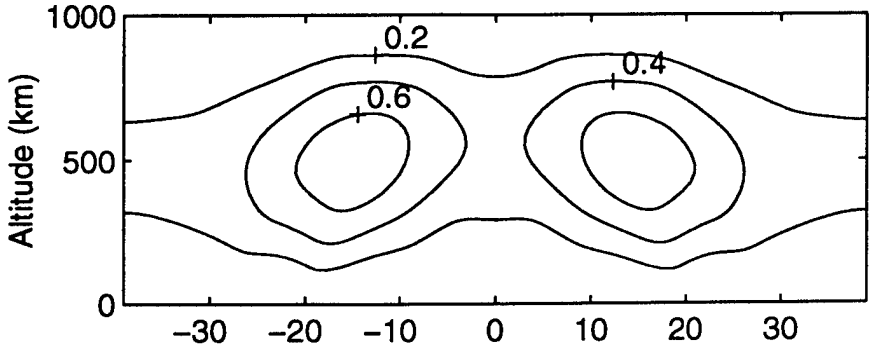

Figure 2: Reconstruction with zero initial guess.

Figure 2 shows a reconstruction that uses no initial guess. Because of the geometry of the IT system, and the fact that very little a priori information is used in the reconstruction

algorithm, the reconstruction of Figure 2 has very poor vertical resolution. The reconstruction of Figure 2 contains only a hint of the variation in height of the peak electron density of the original image.

An initial guess was created by averaging the original image in the horizontal direction, then repeating the vertical profile thus obtained at every latitude. In other words, the initial guess varies with altitude but is constant with latitude. There are two different ways of entering an initial guess into the algorithm. The initial guess can be used as the starting point for the iteration, or the initial guess can be subtracted from the data. Both of these possibilities will be examined in the paragraphs that follow.

In the absence of round off errors, the CG method converges to the exact solution in the number of iterations equal to the number of pixels in the reconstruction. Therefore, if the number of iterations is sufficiently large, then the starting point for the iteration should make no difference in the final solution. For the example problem, if the initial guess is used as the starting point for the iteration, then the reconstruction is virtually identical to the reconstruction of Figure 2. However, in cases where either the TEC data is extremely sparse, or round off errors interfere with the convergence of the CG algorithm, the starting point for the iteration may make a difference in the final reconstruction.

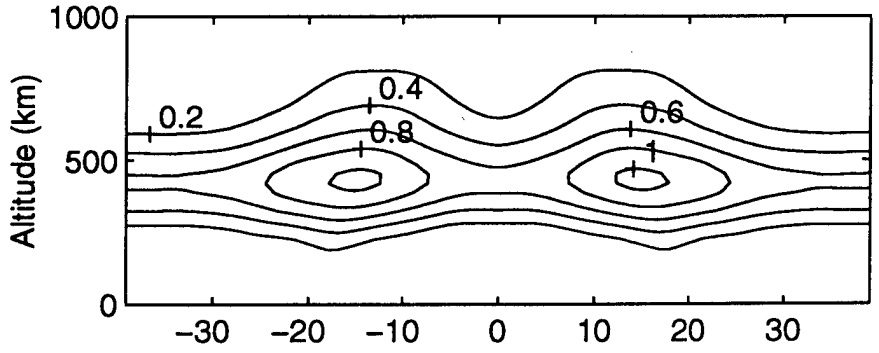

Figure 3: Reconstruction with nonzero initial guess.

The second way of using the initial guess is to subtract it from the data before starting the iteration, then add it back into the solution afterwards. The initial guess becomes the a priori mean for the reconstruction. In this case, the initial guess g is entered into the algorithm by defining

$$b_1 = \begin{bmatrix} b - Ag \\ 0 \end{bmatrix}. \tag{16}$$

The solution is then given by $x + g$. A reconstruction using the initial guess in this way is shown in Figure 3. The maximum electron density of the two peaks in Figure 3 is closer to the correct value than it is for the reconstruction of Figure 2, but the variation in height of the peak electron density is not reconstructed. Figure 3 exhibits an apparent improvement in vertical resolution that is not entirely borne out by comparison with the original image.

A reconstruction using ionosonde information is shown in Figure 4. Note that the vertical resolution is improved for both the bottom side and top side, even though the ionosonde gives information only about the bottom side.

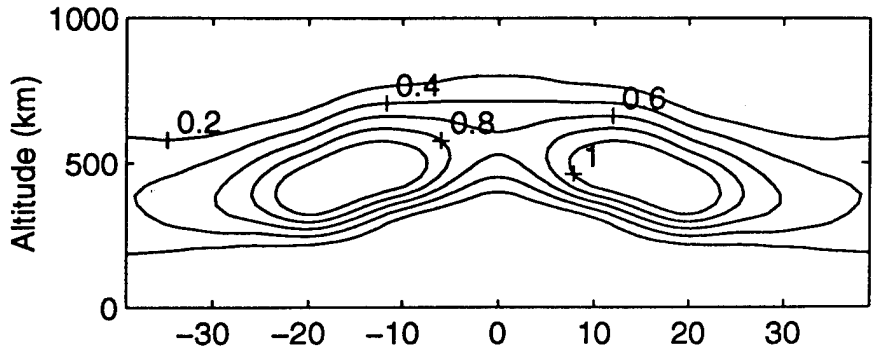

Figure 4: Reconstruction with ionosonde information.

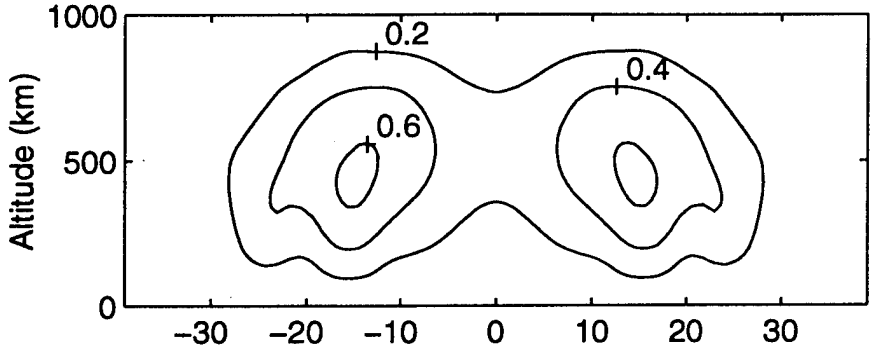

Figure 5: Reconstruction simultaneous with calculation of calibration offsets.

For a real ionospheric tomography system, there is an unknown calibration offset associated with each receiver. This offset is different for different receivers but the same for all data from an individual receiver. It is possible to incorporate the calibration offsets into the reconstruction algorithm and solve for the offsets simultaneously with reconstruction. This is what was done for the reconstruction of Figure 5. Comparing Figure 5 with Figure 2, it is clear that the inclusion of the additional unknowns causes a significant decrease in the quality of the reconstruction.

For the reconstruction of Figure 6, calibration offsets were calculated as for Figure 5, but ionosonde information was also used. The reconstruction of Figure 6 is considerably better than the reconstruction of Figure 5; however, the improvement in top side resolution seen in Figure 4 has been lost due to the inclusion of the additional unknowns in the reconstruction problem.

4 Conclusion

The TEC data collected by ionospheric tomography systems is generally not sufficient to uniquely determine a reconstruction of electron density. Sometimes data from other sources, such as ionosonde data, can be used in addition to TEC data. Even when other sources of information are available, a priori information is generally necessary.

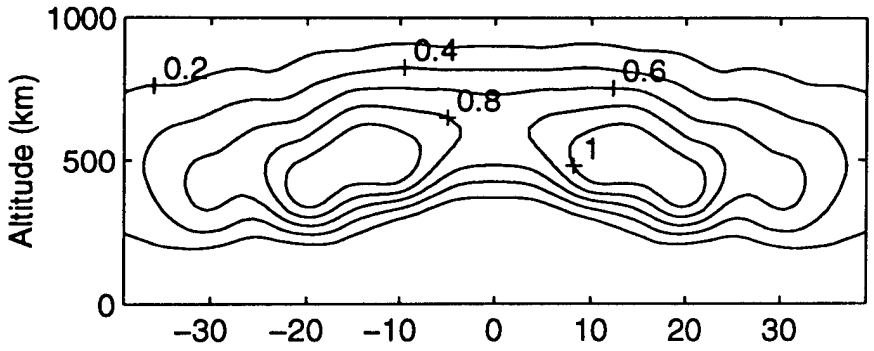

Figure 6: Reconstruction with ionosonde information simultaneous with calculation of calibration offsets.

Many ionospheric tomography algorithms use ionospheric models to supply a priori information. This approach can yield very good reconstructions when the ionospheric electron density is consistent with the a priori information; however, if the a priori information is incorrect, then the reconstructions obtained may be misleading.

An ionospheric tomography algorithm has been presented that does not use ionospheric models in any way; instead, the new algorithm uses very general information about the ionosphere. The new algorithm uses a measure of smoothness to choose one solution from the many solutions that satisfy the TEC data.

Several examples of reconstructions using the new algorithm have been presented. The examples were used to demonstrate the effect of using an initial guess, using ionosonde information, and calculating station offsets.

References

[1] V. E. Kunitsyn, E. S. Andreeva, A. Y. Popov, and O. G. Razinkov, "Methods and algorithms of ray radiotomography for ionospheric research," *Annales Geophysicae*, vol. 13, pp. 1263–1276, Dec. 1995.

[2] M. Kunitake, K. Ohtaka, T. Maruyama, M. Tokumaru, A. Morioka, and S. Watanabe, "Tomographic imaging of the ionosphere over Japan by the modified truncated SVD method," *Annales Geophysicae*, vol. 13, pp. 1303–1310, Dec. 1995.

[3] P. F. Fougere, "Ionospheric radio tomography using maximum entropy: 1. theory and simulation studies," *Radio Science*, vol. 30, pp. 429–444, Mar.–Apr. 1995.

[4] G. C. Fehmers, "A new algorithm for ionospheric tomography," *Proceedings of the International Beacon Satellite Symposium*, pp. 52–55, July 1994.

[5] E. J. Fremouw, J. A. Secan, and B. M. Howe, "Application of stochastic inverse theory to ionospheric tomography," *Radio Science*, vol. 27, pp. 721–732, Sept.–Oct. 1992.

[6] J. R. Austen, S. J. Franke, and C. H. Liu, "Ionospheric imaging using computerized tomography," *Radio Science*, vol. 23, pp. 299–307, May–June 1988.

[7] T. D. Raymund, Y. Bresler, D. N. Anderson, and R. E. Daniell, "Model-assisted ionospheric tomography: A new algorithm," *Radio Science*, vol. 29, pp. 1493–1512, Nov.–Dec. 1994.

[8] E. Sutton and H. Na, "Ionospheric tomography using the residual correction method," *Radio Science*, vol. 31, pp. 489–496, May–June 1996.

[9] E. Sutton and H. Na, "A block iterative algorithm for tomographic reconstruction of ionospheric electron density," *Int. J. Imag. Systems Technol.*, 1996. (in press).

[10] H. Na and H. Lee, "Orthogonal decomposition technique for ionospheric tomography," *Int. J. Imag. Systems Technol.*, vol. 3, no. 4, pp. 354–365, 1991.

[11] E. Sutton and H. Na, "Orthogonal decomposition framework for ionospheric tomography algorithms," *Int. J. Imag. Systems Technol.*, vol. 5, no. 2, pp. 106–111, 1994.

[12] J. A. T. Heaton, S. E. Pryse, and L. Kersley, "Improved background representation, ionosonde input and independent verification in experimental ionospheric tomography," *Annales Geophysicae*, vol. 13, pp. 1297–1302, Dec. 1995.

[13] J. A. Cook and S. Close, "An investigation of TID evolution observed in the MACE '93 data," *Annales Geophysicae*, vol. 13, pp. 1320–1324, Dec. 1995.

[14] J. C. Foster, M. J. Buonsanto, J. M. Holt, J. A. Kobuchar, P. F. Fougere, W. A. Pakula, T. D. Raymund, V. E. Kunitsyn, E. S. Andreeva, E. E. Tereschenko, and B. Z. Khudukon, "Russian-American tomography experiment," *Int. J. Imag. Systems Technol.*, vol. 5, no. 2, pp. 148–159, 1994.

[15] S. E. Pryse, L. Kersley, J. A. T. Heaton, and T. D. Raymund, "Tomographic reconstruction of ionospheric electron density with EISCAT verification," *Proceedings of the International Beacon Satellite Symposium*, pp. 1–4, July 1992.

[16] S. E. Pryse, L. Kersley, D. L. Rice, C. D. Russel, and I. K. Walker, "Tomographic imaging of the ionospheric mid-latitude trough," *Annales Geophysicae*, vol. 11, pp. 144–149, Feb.–Mar. 1993.

[17] K. C. Yeh and T. D. Raymund, "Limitations of ionospheric imaging by tomography," *Radio Science*, vol. 26, pp. 1361–1380, Nov.–Dec. 1991.

[18] H. Na and H. Lee, "Analysis of fundamental resolution limit of ionospheric tomography," *Proc. of the Int'l. Conf. on Acoustics, Speech and Signal Processing*, vol. 3, pp. 97–100, 1992.

[19] H. Na and E. Sutton, "Resolution analysis of ionospheric tomography systems," *Int. J. Imag. Systems Technol.*, vol. 5, no. 2, pp. 169–173, 1994.

[20] H. Na and H. Lee, "Resolution degradation parameters of ionospheric tomography," *Radio Science*, vol. 29, pp. 115–125, Jan.–Feb. 1994.

[21] H. Na, B. Hall, and E. Sutton, "Ground station spacing effects in ionospheric tomography," *Annales Geophysicae*, vol. 13, pp. 1288–1296, Dec. 1995.

[22] T. D. Raymund, S. J. Franke, and K. C. Yeh, "Ionospheric tomography: Its limitations and reconstruction methods," *J. Atmos. Terr. Phys.*, vol. 56, pp. 637–657, May 1994.

[23] E. Sutton and H. Na, "Comparison of geometries for ionospheric tomography," *Radio Science*, vol. 30, pp. 115–125, Jan.–Feb. 1995.

[24] G. C. Fehmers, "An efficient optimization algorithm for ill posed linear and discrete inverse problems," *Inverse Problems*, (to be published).

[25] K. E. Atkinson, *An Introduction to Numerical Analysis*, ch. 8. New York: Wiley, 1978.

[26] A. C. Kak and M. Slaney, *Principles of Computerized Tomographic Imaging*, ch. 7. New York: IEEE Press, 1988.

A Localized Space-Frequency Algorithm for Computerized Ionospheric Tomography

Helen Na and Chaitali Biswas

Electrical Engineering Department
University of California, Los Angeles
Los Angeles, California 90095–1594

Abstract

Ionospheric tomography is a rapidly developing technique for imaging ionization distributions. Due to the system configuration, the resolving capability of these systems is still limited. A number of reconstruction algorithms have been developed which strive to form high resolution images by enhancing the available data with information provided by model ionospheres. This paper presents a new Fourier domain algorithm for ionospheric tomography which uses unique characteristics of ionospheric spectra to enhance the reconstructions. Unlike most model based algorithms, this solution is not limited to a linear combination of model ionospheres and data. This algorithm also uses a localized approach which enables reconstructions of varying resolution in different regions of the ionosphere.

I. Introduction

A recent development in the area of ionospheric electron density distribution measurement, Computerized Ionospheric Tomography (CIT) holds considerable potential in applications ranging from broadcast communications and surveillance to plasma science and radio astronomy. Imaging of the electron density distribution over a certain geographical region in the vertical plane [Austen at al., 1988; Fougere 1995; Fremouw et al., 1992; Kronschnabl et al., 1995; Na and Lee, 1991; Pryse and Kersley, 1992; Sutton and Na, 1995; Raymund 1994], is performed by an Earth-Satellite data acquisition system shown in Figure 1. The satellite transmits two signals, at 150 and 400 MHz respectively, as it passes overhead at an altitude of approximately 1000km. These signals, received simultaneously by the chain of ground stations in the same vertical plane, contain information regarding the electron density along each raypath through the ionosphere and are known as Total Electron Content (TEC) measurements.

Mathematically, each TEC may be represented as the line integral of electron density N_e along a raypath P between satellite position s_i and ground station g_j :

$$TEC(s_i g_j) = \int_{x \epsilon P} N_e(x) \; dx \tag{1}$$

This equation conforms to the expression for individual projection samples according to the Radon Transform [Kak and Slaney 1988] of conventional tomography. Grouping TEC samples from ray paths of various stations that are inclined at a specific angle θ, yields a pseudo

tomographic projection set P_θ as shown in Figure 1. By the Central Slice Theorem (CST) [Kak and Slaney 1988], the one-dimensional FFT of P_θ corresponds to a linear slice in the two-dimensional FFT of the spatial image inclined at θ.

Due to geometric constraints of the imaging system such as the continuity of the ionospheric shell, the curvature of the earth and the limited number of ground stations, it is not possible to record TEC measurements along the horizontal [Yeh and Raymund, 1991; Raymund et al., 1994; Na and Sutton, 1994; Na and Lee, 1994; Sutton and Na, 1995]. This results in samples and even entire projection sets missing along the vertical direction from the two dimensional Fourier spectrum of the image. Specifically, it results in a double missing cone as shown in Figure 2. The reconstruction process, thus, involves calculation of extrapolated values, often based on a priori information, in this missing cone region, to obtain an enhanced spectrum and its image.

The Fourier domain has natural characteristics that are very well suited for the problem of ionospheric tomography. The above mentioned relationship between total electron content data, and the two-dimensional spectrum of the ionospheric distribution enables a clear separation between regions where adequate information has been measured and regions where a priori information is needed. This separation cannot be made in the spatial domain. Furthermore, spectra of greatly varying ionospheric distributions have similar underlying characteristics. These characteristics can be utilized to enhance ionospheric tomography reconstructions.

This paper presents a Fourier domain algorithm that uses a localized approach to enhancement. By expanding the measured data into the four-dimensional space-frequency domain, the

spectral content is localized. The estimation of missing information can then be performed using only local spectral characteristics. Further localization is made possible by selecting a priori information to be used for enhancement in each local region based upon only local spectral characteristics.

The a priori information used in this algorithm is derived from a database of model ionospheres. However, unlike many other model based approaches, the solution is not constrained to lie within the space defined by the models. This algorithm thus permits solutions which are not merely the result of linear combination of model ionospheres, hence enabling a robust balance between data and model information. The localization in this algorithm not only enhances the reconstructions, but provides a method for reconstructing images of varying resolution in different regions of the ionosphere.

II. Direct Fourier Method

Fourier methods are based upon the central slice theorem of tomography [Kak and Slaney 1988]. Consider the ionospheric tomography system shown in Figure 1. Total electron content data is acquired for every propagation path between each satellite location and ground station. Tomographic projections can be formed by grouping the TEC data according to the angle of the propagation paths. The central slice theorem relates the Fourier transform of these projections to the two-dimensional Fourier transform of the electron density distribution which is being reconstructed.

Let $p_\theta(t)$ be a projection of the electron density distribution at angle θ, or the collection

of TEC data with propagation paths at an angle θ. Let $f(x,y)$ represent the two-dimensional electron density distributions, or the image to be reconstructed. Now consider the Fourier transform of the $p_\theta(t)$ denoted $P_\theta(f)$.

$$P_\theta(f) = \int_{-\infty}^{\infty} p_\theta(t) e^{-jwt} dt \tag{2}$$

Each projection can be expressed as a line integral through the electron density distribution, using a rotated coordinate system.

$$p_\theta(t) = \int_{-\infty}^{\infty} f(t,s) ds \tag{3}$$

The coordinate systems are related by the following matrix.

$$\begin{bmatrix} t \\ s \end{bmatrix} = \begin{bmatrix} \cos\theta & \sin\theta \\ -\sin\theta & \cos\theta \end{bmatrix} \begin{bmatrix} x \\ y \end{bmatrix} \tag{4}$$

By substituting Equation 3 into Equation 2, the Fourier transform of a projection can be written in terms of the electron density distribution.

$$P_\theta(f) = \int_{-\infty}^{\infty} \left[\int_{-\infty}^{\infty} f(t,s) ds \right] e^{-jwt} dt \tag{5}$$

Using the relationship in Equation 4, this can be transformed into the original (x,y) coordinate system.

$$P_\theta(f) = \int_{-\infty}^{\infty} \int_{-\infty}^{\infty} f(x,y) e^{-j2\pi w(x\cos\theta + y\sin\theta)} dx dy \tag{6}$$

The two-dimensional Fourier transform of the electron density distribution has a similar form.

$$F(u,v) = \int_{-\infty}^{\infty} \int_{-\infty}^{\infty} f(x,y) e^{-j[ux+vy]} dx dy \tag{7}$$

By comparing Equation 6 to Equation 7, it can be shown that each projection spectrum is one slice of the image spectrum.

$$P_\theta(f) = F(w\cos\theta, w\sin\theta) \tag{8}$$

This relationship is depicted in Figure 3.

The fundamental Fourier domain reconstruction algorithm, called the direct Fourier method, applies the central slice theorem to the Fourier transform of each projection. The result is the two-dimensional spectrum of the image. An inverse two-dimensional Fourier transform produces the image.

In ionospheric tomography, the angles of the propagation paths are restricted by physical limitations of the system. Therefore, slices of the image spectrum are correspondingly restricted creating a missing cone of information, as shown in Figure 3. The effect in the final image is shown in Figure 4 and Figure 5. Figure 4 shows the original image and Figure 5 shows the image reconstructed using the direct Fourier method from data that was restricted to a 120° range. As with other ionospheric tomography algorithms, clearly enhancement is needed in order to estimate the missing information.

III. Localized Space-Frequency Algorithm

The new algorithm, based upon the Direct Fourier Method, uses a localized reconstruction process and Fourier domain feature extraction for incorporation of local a priori information from a database of model ionospheres. This algorithm has several unique features. First, the emphasis on local processing and local a priori information enables the algorithm to be

specialized in each region of the ionosphere. This would, for example, permit varying degrees of resolution to be specified for each region based upon the requirements of the particular application. Furthermore, the estimation of the missing information is enhanced by utilizing only local spectral measurements and features. This algorithm also exploits the unimodal characteristics of the ionospheric spectra for classification of a priori information.

Reconstruction is achieved in this algorithm by alternately processing the signal in the spectral and spatial domains for each region of the image. The iterative nature of the algorithm allows incorporation of some amount of a priori information in each stage of the recovery process. This amount can be regulated both according to the iteration number and location of the region of interest. The above situation ensures a convergent balance between recorded data and model, thus allowing for reliability and robustness of solution.

The localized space-frequency algorithm expands the two-dimensional missing cone spectrum, obtained from the data, into a four-dimensional space-frequency domain. This space-frequency domain is a four-dimensional extension of the two-dimensional time-frequency space. Two-dimensional time-frequency distributions, provide information on the frequency distribution of a signal over time, unlike Fourier domain spectra which only describe the net frequency content [Boashash 1991], and thus, by definition assumes knowledge of signal over time $t \in (-\infty, \infty)$.

The time-frequency representation of one dimensional signals is analogous to a musical score where notes, i.e. frequencies, are shown as a function of when they are to be played, i.e. time. Time-frequency analysis is used for a wide range of signal processing applications such as in

filtering of harmonics in speech signals. Extending the concept to two-dimensional signals such as images, simultaneous representation of energy distribution in the two spatial and two spectral dimensions can be defined in a four-dimensional information space. Energy distribution at a fixed frequency occurring at various spatial locations within the image can now be individually identified and vice-versa. Localization thus achieved, aids in selective modification of important image features based on their spectral content.

Given the limited quantity of reliable information in the recorded data, preservation of data accuracy in the reconstruction process is crucial to the success of the algorithm. The localization property of four-dimensional space-frequency domain allows an extra level of information to be extracted from the data. Consider the known portion of the spectrum. This is simply the measured data in a different domain. The four-dimensional space-frequency expansion stretches the measured data by providing information on a relationship of the data to each spatial location. This can be likened to knowing not only which colors exist in a photograph, but where that color exists.

Several two-dimensional time-frequency distributions exist which can be extended to four-dimensions including the Wigner-Ville, and the Short-Time Fourier Transform (STFT) [Boashash 1991]. In this paper, we present an algorithm based upon a simplified version of the four-dimensional extension of the Short-Time Fourier Transform. This four-dimensional extension will be referred to as the Limited-Area Fourier Transform (LAFT).

The idea behind Limited Area Fourier Transform is to isolate regions of the image and

investigate spectral properties of the same. A simple rectangular windowing function $w_{a,b}(x,y)$ is used to isolate an $l \times l$ section of the image centered at $(al + l/2, bl + l/2)$ so that the whole image can be selectively partitioned into $(N/l)^2$ partial images each denoted by the ordered pair (a,b). Thus the partial image $f_{a,b}(x,y)$ can be expressed in terms of the original image $f(x,y)$ as :

$$f_{a,b}(x,y) = f(x,y) \times w_{a,b}(x,y) \tag{9}$$

Using rectangular windowing, the two-dimensional Fourier transform of the window function in the center would be :

$$W_{0,0}(u,v) = \int_{-l/2}^{l/2}\int_{-l/2}^{l/2} e^{-j2\pi\left[\frac{ux+vy}{N}\right]}\ dxdy \ = \ l^2 sinc\left(\frac{ul}{N}\right) sinc\left(\frac{vl}{N}\right) \tag{10}$$

In shifting the window to extract the block (a,b) an exponential term gets multiplied with equation 10 so that :

$$W_{a,b}(u,v) = e^{-j2\pi\left(\frac{ua+vb}{N}\right)l} W_{0,0}(u,v) \tag{11}$$

and a partial spectrum can be represented as :

$$F_{a,b}(u,v) = F(u,v) * W_{a,b}(u,v) \tag{12}$$

If a missing cone of θ degrees appears in the whole spectrum then a similar missing cone appears in all the partial spectra with the cone edges marginally blurred because of the sinc convolution.

This transform was chosen because its method of localization in the image domain can be easily matched to desired regions of the ionosphere. According to basic STFT, the complete

time-frequency representation of a signal involves window shifts of unit distance along the time axis to estimate instantaneous frequencies. As a two-dimensional version of STFT, LAFT involves single pixel shifts of the square area window function along either axis for computing successive values in the localized four-dimensional information space. In order to reduce the number of computations without significant loss of resolution, the experimental version of LAFT was implemented using a sub-sampled version of the full LAFT such that the set of partial images were formed by non overlapping window functions.

The image reconstructed from the direct Fourier method is the starting point for the localized space-frequency algorithm. This image is segmented into subregions by the LAFT. Each subregion and its Fourier transform are then processed individually. A modified iterative Gerchberg-Papoulis extrapolation procedure is used to estimate the missing information in each local spectrum. Local a priori information is incorporated into the reconstruction process in this modified Gerchberg-Papoulis procedure. Once the localized regions have been reconstructed, the final image is formed by reassembling the appropriate segments of the image region.

The original Gerchberg-Papoulis extrapolation procedure is an iterative enhancement technique which uses minimal a priori information, requiring only the spatial limits of the image [Gerchberg 1974, Papoulis 1975]. Figure 6 outlines one iteration of the Gerchberg-Papoulis procedure and the modified Gerchberg-Papoulis procedure. This process iterates between the spatial and Fourier domains enforcing spatial limits in the spatial domain and the values obtained from the measured data in the Fourier domain. In the Fourier domain, the region that was

originally unknown is replaced in each iteration by the values estimated through the previous iteration. Because CIT systems are severely underdetermined, Gerchberg-Papoulis extrapolation does not incorporate sufficient a priori information for image enhancement. In order to improve the reconstruction, we modify the procedure to incorporate local a priori information provided by model ionospheres. In the Fourier domain, instead of simply replacing the known region with the original measured values, we also alter the estimated region of the image by replacing the estimated values with a weighted sum of estimated values and values obtained from the 'best fit' a priori spectrum. A convergent balance between reliability of data and a priori support is eventually achieved.

The 'best fit' local a priori spectrum is identified by examining a two-dimensional feature space. A database of model ionospheres is generated from the IRI-90 model. Each model ionosphere is segmented into subregions by the LAFT. Since spectra of local regions of the model ionospheres have a unimodal distribution, two features of each local spectrum are used to characterize the spectrum, as shown in Figure 7. The first feature is the magnitude of the central peak and the second feature is the transverse diameter of the peak at a given height. These correspond to the first and second moments of the distribution. For each local ionospheric region, the database is reduced to a collection of feature pairs: (magnitude, diameter).

A two-dimensional plot of points, each representing an image or sub-image forms a feature space. A sub-image at block x-y is formed by extracting the region of the whole-image that occurs within the tile occupying the xth row and yth column of the image grid. A priori information for

each local region is represented by one plot of the appropriate two-dimensional feature space. Two sample feature space plots generated from 300 model images for two different locations of the same image are shown in Figure 8. The plot on the left for block 0–0, which corresponds to a region of low electron density and minor variations in distribution patterns, shows smaller magnitude and spectral lobe diameters than the plot for block 2–3 which corresponds to a region of high electron content and activity.

The image points in each feature space plot which lie in close proximity in a local area form a cluster. Clustering refers to the operation of nominating a representative of each cluster to form a higher level database of feature points for the feature identification process. Clustering thus reduces the initial feature space to a group of possible representative models for each ionospheric image region, each characterized by a different feature pair: (magnitude, diameter).

The 'best fit' a priori spectrum is determined by performing feature extraction on the localized spectrum, prior to the extrapolation process, to identify its feature pair, (magnitude, diameter). The feature pair is then compared to the a priori feature space and a 'best fit' a priori subregion is formed through a weighted linear combination of the representative local model subregions. The weights are determined by the distance in the feature space to each cluster point. The 'best fit' a priori spectrum is used in the modified Gerchberg-Papoulis to improve estimation of the missing region in each iteration.

A flowchart of the complete localized space-frequency algorithm is shown in Figure 9. First, the central slice theorem is used to form the missing cone spectrum of the complete image. The

complete image without enhancements is obtained through an inverse Fourier transform. This image is segmented into several subregions. Each subregion is then processed individually. Feature extraction is performed on each partial spectrum and the 'best fit' local a priori partial spectrum is identified. The modified Gerchberg-Papoulis extrapolation process is used to estimate the missing spectral information. This process converges upon the enhanced reconstruction of each subregion. These reconstructions are recombined to form the final image.

IV. Results

This algorithm was tested using a database of 300 model ionospheres generated using IRI-90. The image was subdivided into sixteen subregions of equal size. Feature sets were formed from the 300 model ionospheres for each of the 16 subregions. Clustering showed that each subregion could be reasonably represented using 10 to 15 representative feature pairs and model subregions.

Figure 4 shows the test image. It was assumed that data was available covering projection angles from -60° to 60°, that is the imaging system introduced a missing cone of semivertical angle 30°. The test image was created by a nonlinear combination of two dissimilar model images simulated for the same observation site. It was ensured that no single image from the database or linear combinations thereof would be sufficient to uniquely characterize the test image. The composite test figure represents a partially perturbed ionosphere. Creation of a missing cone in its spectral domain makes the test image-model data base relationship highly non-linear. Hence it is possible to claim that the test image is an independent representative of ionospheric conditions above the same location as the model database.

Figure 5 shows the reconstruction using the direct Fourier method without any a priori information or extrapolation. In other words, this is the information available from only the data. Figure 10 shows the reconstruction using the localized space-frequency algorithm. In the modified Gerchberg-Papoulis process, the weighting between the a priori partial spectrum and the estimated partial spectrum was chosen to be even, i.e. 50% of each was used. Figure 10 was obtained using 10 iterations of the modified Gerchberg-Papoulis process on each of the 16 subregions.

For qualitative comparison, a set of three reconstructions is presented in Figure 11. Figure 11a shows the original test image, Figure 11b shows the image with a 30° missing cone in its spectrum and Figure 11c shows a reconstruction with 30% a priori information. It was observed that beyond 30%-40% model based a priori information lay a region of diminishing returns. This is substantiated by the graph shown in Figure 13. Comparison of Figure 11(a) and (b) show a general lowering and smoothing of the two peak electron concentration zones and formation of a ridge like structure in the high altitude regions (700–1000 km). There appear to be three distinct centers of electron concentration in the latter image. Figure 11(c) shows a considerable improvement from 11(b). The two peak structure is restored, the high altitude ridge obscured and the general shape of the low altitude electron distribution contours partially recovered. Note also the relative loss of information in the lower left hand corner of 11(c). This can be attributed to a mismatch of test and model blocks resulting from misidentification at this point. The overall contour shapes are significantly restored in Figure 11(c).

The response of the space-frequency algorithm to noise corrupted data was tested by creating an image corresponding to projection sets whose samples were randomly corrupted by "measurement" noise up to 10% signal strength. Noise corruption of random samples in the projection sets amounts to linear ridges and furrows on the two-dimensional backprojected image. Figures 12(a), (b), (c) and (d) show the data image with a spectral missing cone and corrupted by noise, followed by reconstructions with 30% and 50% a priori information, respectively. These show that the space-frequency algorithm is able to extract adequate quantities of signal information for identifying related, uncorrupted, a priori information. Influence of this a priori information is demonstrated in the two successive reconstructions. The reconstruction using 50% a priori reconstruction is a better approximation of the original than the one using 30% a priori information. This example demonstrates that the process of local spectral identification of a priori data is relatively immune to high levels of noise corruption.

A third set of images were used for quantitative estimation of the algorithm performance. Figure 13 shows a composite plot of average mean square error (mse) for reconstructions using 0% – 90% a priori information and 1 to 10 iterations. It can be seen that significant improvement is obtained as the percentage of a priori information is increased from 0% to 40% or 50%. However, the improvement saturates at that point. For 30% or higher amounts of a priori information, the reconstructions converge within 10 iterations.

V. Conclusions

This paper has presented a localized space-frequency algorithm for ionospheric tomography.

This algorithm enables local characteristics of the ionosphere to be used for image enhancement and exploits the features of the local spectra for selection of a priori information. Because of the way in which a priori information is incorporated in this routine, reconstructions are not restricted to a space defined by the a priori information. The localization in this algorithm is determined by the segmentation of the image region. This can be based upon the characteristics of a rough reconstruction or a priori information. Because of the localized processing, this approach may be useful for imaging ionospheric conditions with significant local irregularities.

There are a number of parameters in this algorithm which govern its performance. These include the weighting given to a priori information, the number of iterations, and most importantly, the selection of the subregions. This paper has discussed the effects of the first two parameters. Further investigations are needed to analyze the effects of varying subregion selection.

The computational requirements of this algorithm are based upon the number of subregions selected. However, since the processing of each subregion is entirely independent of other subregions, the reconstructions can be performed in parallel. Also, calculation of the feature spaces from model ionospheres is only performed once for any given segmentation. Finally, although this algorithm is an iterative approach, it has been shown that fewer than 10 iterations are needed for typical reconstructions.

VI. Acknowledgments

This material is based upon work supported by the National Science Foundation under grant ATM-9419552 and the Office of Naval Research under grant N00014–95–1–0850.

VII. References

Austen, J. R., S. J. Franke, and C. H. Liu, Ionospheric imaging using computerized tomography, *Radio Science*, 23(3), 299–307, 1988.

Boashash, B., Time-Fequency Signal Analysis,*Advances in Spectrum Analysis and Array Processing*, 1(9), 418–517, Prentice Hall, 1991.

Fehmers, G. C., A new algorithm for ionospheric tomography, *Proc. of the Beacon Satellite Symposium*, (Aberystwyth, Wales, July 1994), 52–55, 1994.

Fougere, P. F., Ionospheric radio tomography using maximum entropy: 1. theory and simulation studies, *Radio Science*, 30(2), 429–444, 1995.

Fremouw, E. J., J. A. Secan, and B. M. Howe, Application of stochastic inverse theory to ionospheric tomography, *Radio Science*, 27(5), 721–732, 1992.

Fremouw, E. J., J. A. Secan, R. M. Bussey, and B. M. Howe, A status report on applying discrete inverse theory to ionospheric tomography, *Int'l. J. Imag. Systems & Technol.*, 5(2), 97–105, 1994.

Gerchberg, R.W., Super-resolution through Error Energy Reduction, *Opt.Acta.*, 21, 709–717, 1974.

Kak, A.C., and Slaney, M.,*Principles of Computerized Tomographic Imaging, IEEE, NY*, 1988.

Kronschnabl, G. R., G. S. Bust, J. A. Cook, and C. J. Vasicek, Mid-america computerized ionospheric tomography experiment (MACE '93), *Radio Science*, 30(1), 105–108, 1995.

Na, H. and Lee, H., Orthogonal decomposition technique for ionospheric tomography, *Int'l. J. Imag. Systems & Technol.*, 3(4), 354–365, 1991.

Na, H. and Lee, H., Resolution degradation parameters of ionospheric tomography, *Radio Science*, 29(1), 115–125, 1994.

Na, H., Shen, J., and Lee, H., A Fourier Domain Technique for Ionospheric Tomography, *Radio Science*, 30(3), 747–754, 1995.

Na, H. and Sutton, E., Resolution analysis of ionospheric tomography systems, *Int'l. J. Imag. Systems & Technol.*, 5(2), 169–173, 1994.

Papoulis, A., A New Algorithm in Spectral Analysis and Bandlimited Extrapolation, *IEEE Trans. Circuits and Systems*, 22, 735–743, 1975.

Pryse, S. E. and L. Kersley, A preliminary test of ionospheric tomography, *J. Atmos. & Terr. Physics*, 54(7/8), 1007–1012, 1992.

Raymund, T. D., Ionospheric tomography algorithms, *Int'l. J. Imag. Systems & Technol.*, 5(2), 75–85, 1994.

Raymund, T. D., . S. J. Franke, and K. C. Yeh, Ionospheric tomography: its limitations and reconstruction methods, *J. Atmos. & Terr. Physics*, 56(5), 637–757, 1994.

Rothleitner, W., Leitinger, R., Kirchengast, G., Using the Fourier domain for reconstruction in ionospheric tomography: a discussion, *Proc. 1994 Beacon Satellite Symposium, Aberystwyth, Wales, July 1994*, 56–59, 1994.

Sutton, E. and H. Na, Comparison of geometries for ionospheric tomography, *Radio Science*, 30(1), 115–125, 1995.

Sutton, E. and H. Na, Ionospheric tomography using the residual correction method, *Radio Science*, 1996 (in press).

Yeh, K. C. and T. D. Raymund, Limitations of ionospheric imaging by tomography, *Radio Science*, 26(6), 1361–1380, 1991.

VIII. List of Figures

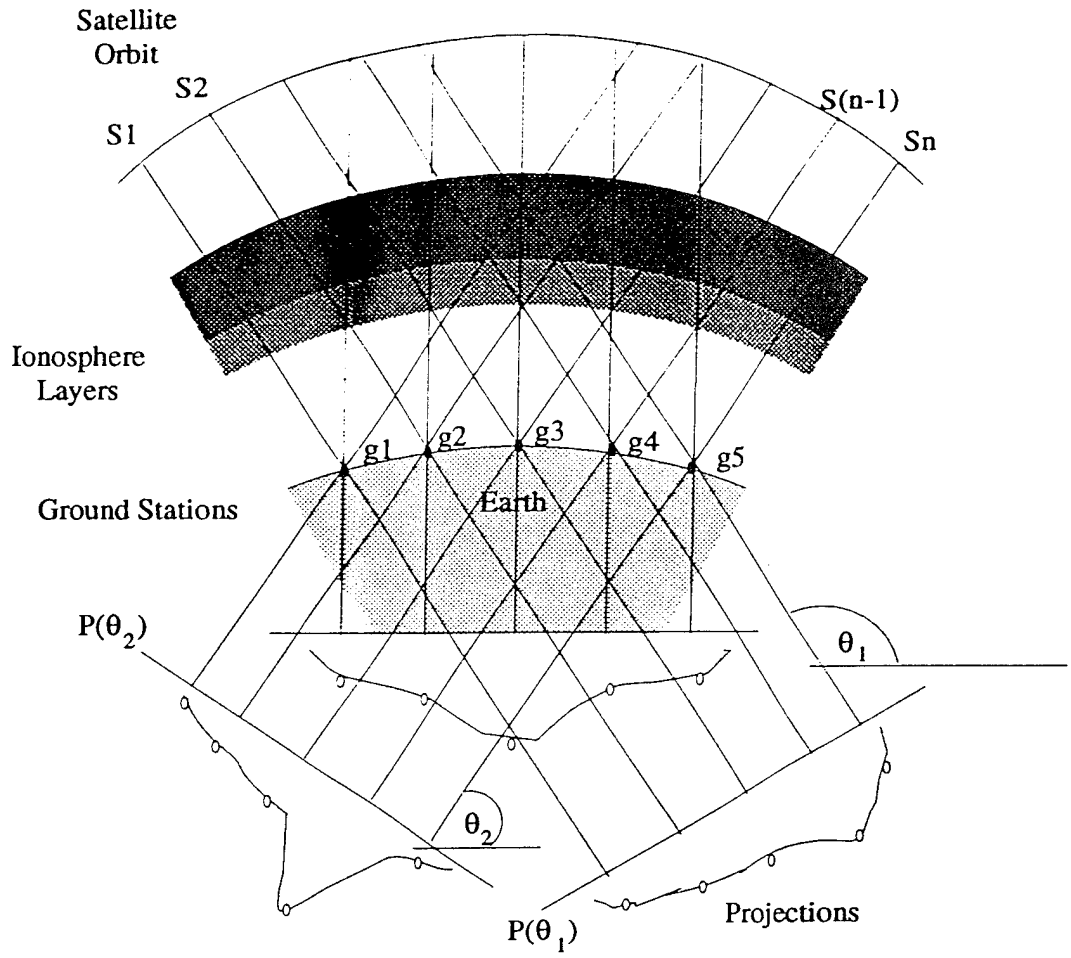

Figure 1. The computerized ionospheric tomography imaging system.

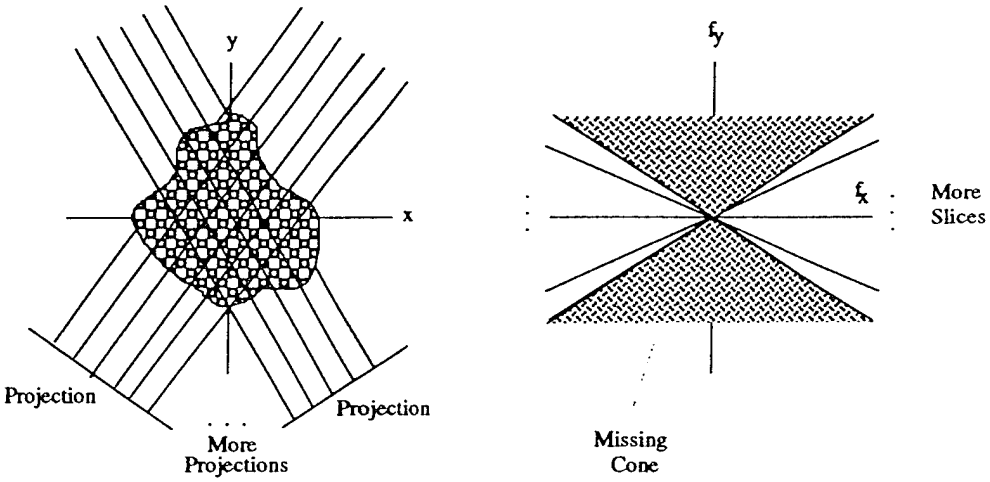

Figure 2. The missing cone problem of CIT.

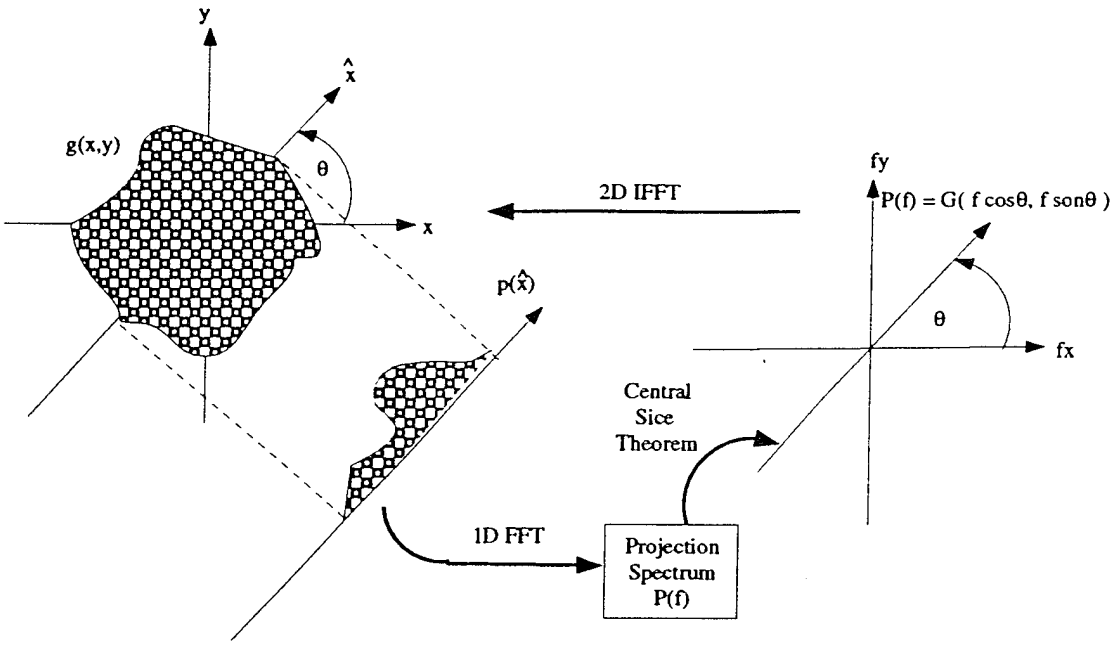

Figure 3. Diagrammatic representation of the central slice theorem that relates 1D projections to the 2D Fourier spectrum.

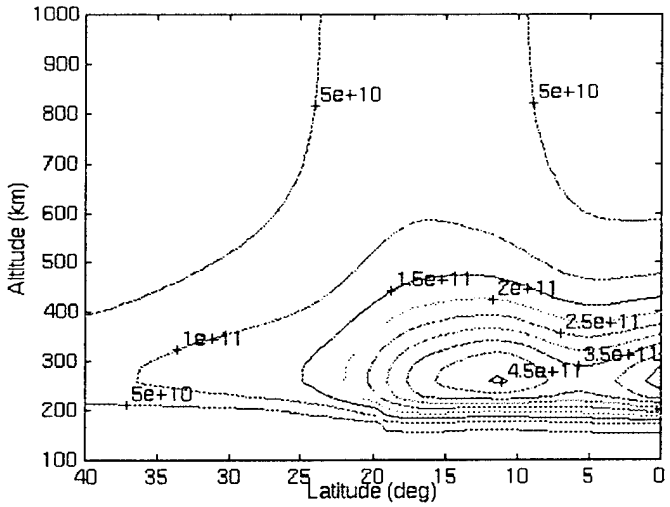

Figure 4. Contour plot of electron density distribution in original image based on IRI-90 model.

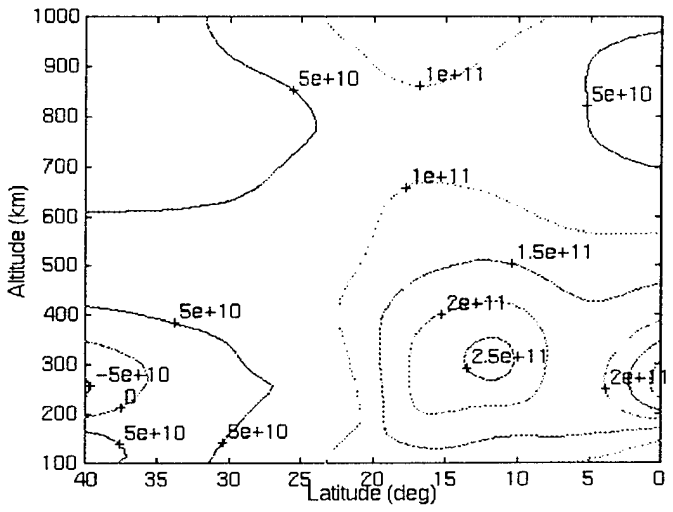

Figure 5. Contour plot of electron density distribution in missing cone image with semivertical angle 30'.

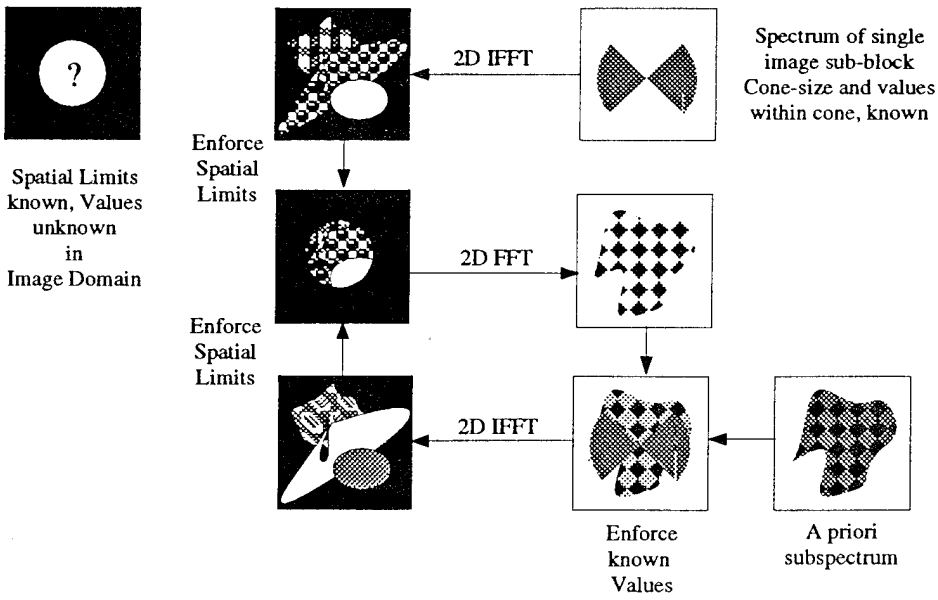

Figure 6. The modified Gerchberg-Papoulis extrapolation algorithm.

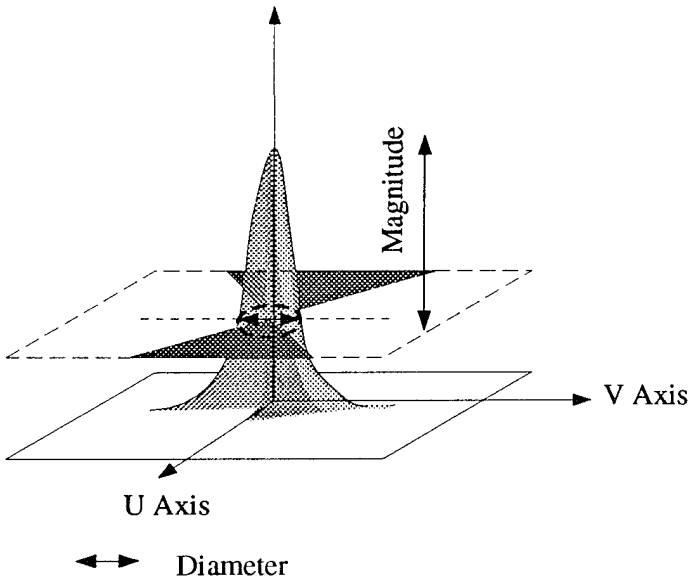

Figure 7. Features used for a priori spectrum identification.

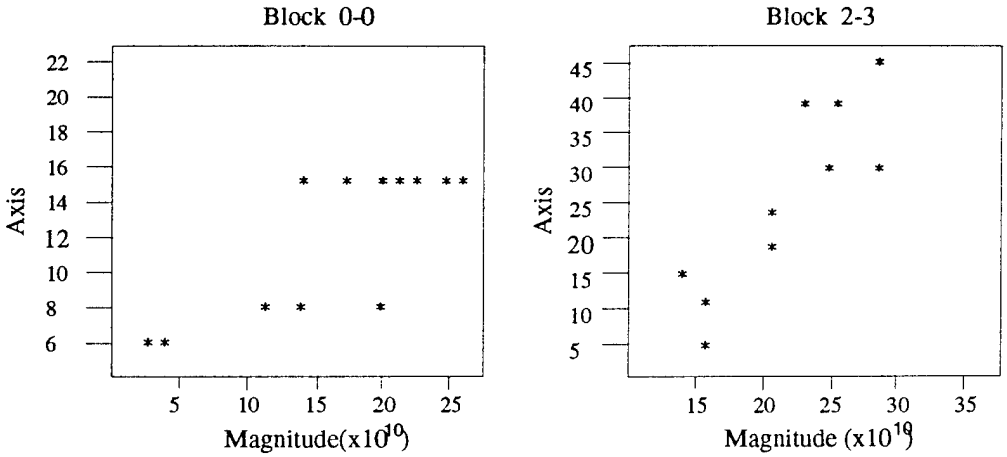

Figure 8. Sample feature plots for two different regions of same ionospheric image.

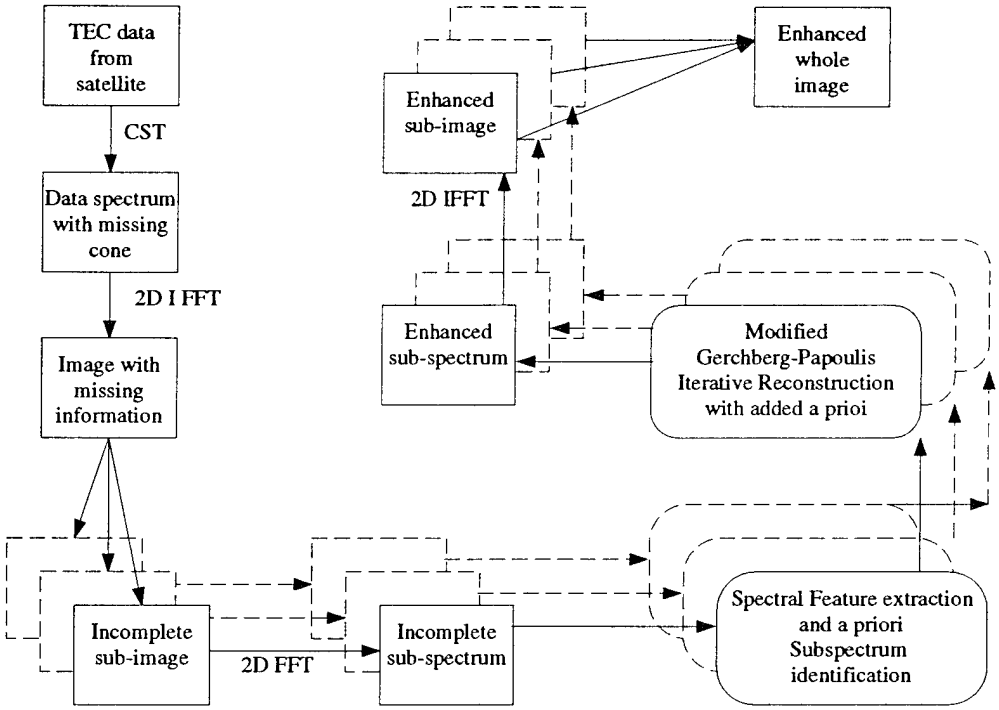

Figure 9. The Space-Frequency Reconstruction Algorithm.

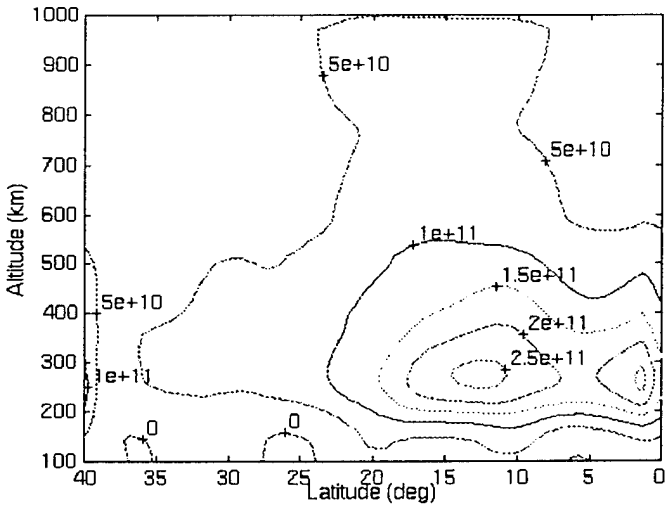

Figure 10. Contours of image recosntructed from Figure 5 using 50% a priori and 10 iterations.

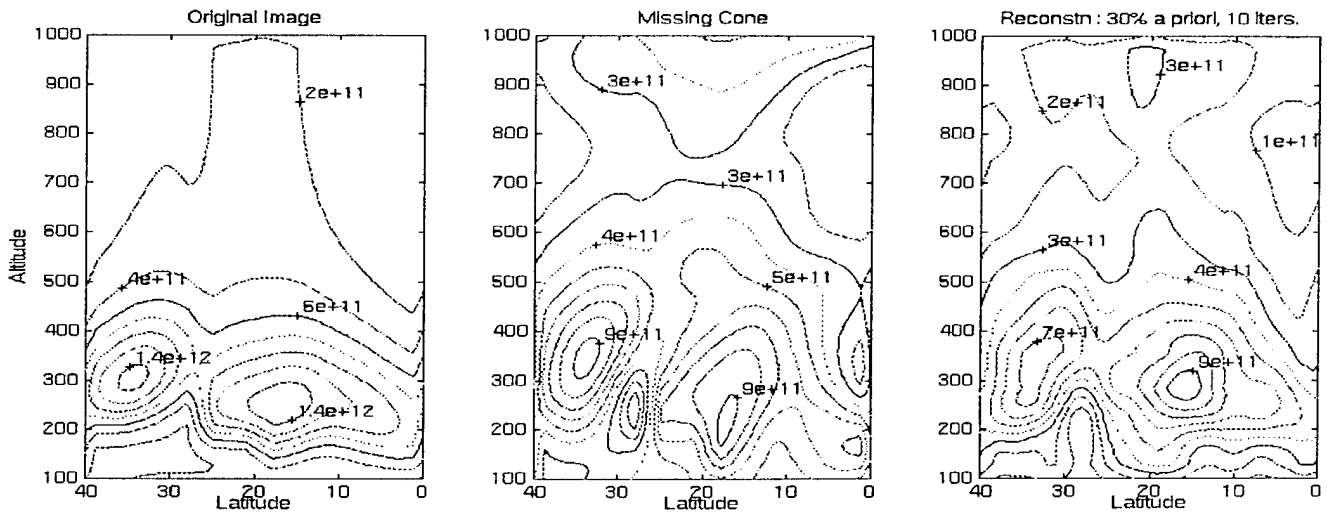

(a) (b) (c)

Figure 11. (a) Original test image with contours. (b) Missing cone test image contours. (c) Reconstruction of test image with 30% a priori information and 10 iterations.

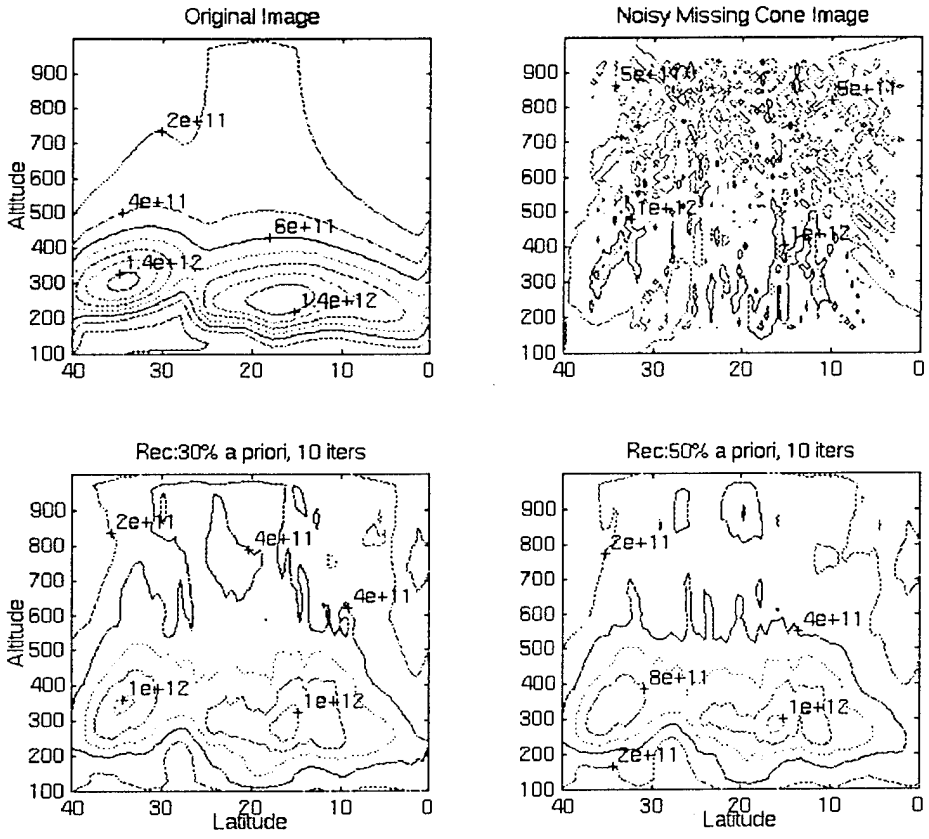

Figure 12. Results of reconstruction using a missing cone image with measurement noise..

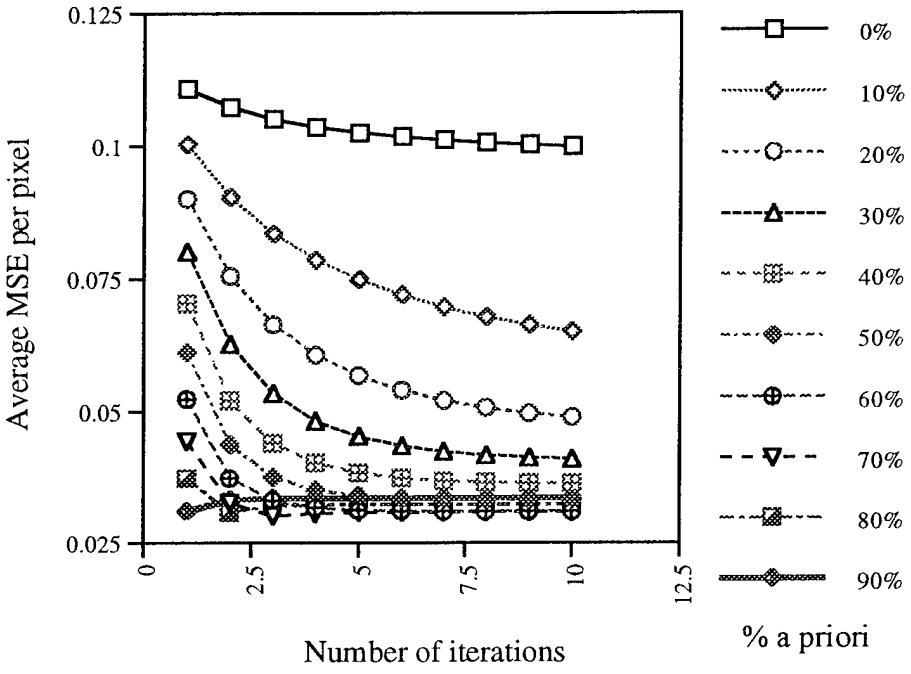

Figure 13. Average mean square error per pixel for reconstruction using various levels of a priori and number of iterations.

STATIC TOMOGRAPHIC RECONSTRUCTION OF THE TIME VARYING IONOSPHERE

Eric Sutton and Helen Na

Department of Electrical and Computer Engineering
University of Iowa
Iowa City, Iowa 52242

ABSTRACT

An image of electron density in a vertical slice through the ionosphere can be created using tomographic techniques. An ionospheric tomography system consists of a satellite and several ground stations. Ionospheric electron density can change significantly during the time it takes to collect enough data for one image. In many other applications of tomography, motion of an object in the source image produces obvious artifacts in the reconstruction such as streaking along object edges. For ionospheric tomography, the effects of motion in the source image are less obvious but nevertheless cause serious errors in the reconstruction. This paper discusses the effects of motion in the ionosphere on static ionospheric tomography reconstructions, and suggests ways to detect that a reconstruction has been corrupted by motion in the source image. Several simulated examples are presented using two different ionospheric tomography reconstruction algorithms.

1. INTRODUCTION

Ionospheric tomography (IT) is a technique that is used to reconstruct images of ionospheric electron density [1, 2]. An IT system consists of a satellite in polar orbit and several ground stations located along a line of longitude underneath the orbit of the satellite. Using the differential Doppler technique, total electron content (TEC) data are obtained along paths between the satellite and the ground stations. TEC is the integral of electron density, so tomographic techniques are used to reconstruct an image of ionospheric electron density in a vertical plane that includes the satellite orbit and the ground stations. The principal difficulty associated with IT is that the TEC data do not form a complete set of projections of the source image [3, 4]. Therefore all practical IT algorithms use *a priori* information to supplement the information contained in the TEC data.

Another source of information that can be used to supplement TEC data is ionosonde data. An ionosonde is essentially a one dimensional radar looking straight up. The ionosonde gives electron density values in a vertical line above the location of the ionosonde up to the altitude of the maximum electron density. The ionosonde only gives information on the bottom side of the ionosphere and only over a very limited area.

One of the sources of errors for IT systems is movement in the ionosphere during data collection. A typical IT system tracks a satellite through about 70° of latitude. A satellite at an altitude of 1000 km takes approximately 20 minutes to traverse 70°. Significant motion in the ionosphere can occur during the 20 minutes required to collect data for a single IT reconstruction. The currently accepted practice in IT is to assume that all data are collected simultaneously and to perform the reconstruction as if the source image were not varying [3, 4]. However, movement in the ionosphere during data collection is a significant contributor to errors in IT reconstructions. This paper will examine and characterize the errors that occur in static IT reconstructions due to movement in the ionosphere.

2. IONOSPHERIC TOMOGRAPHY ALGORITHMS

Ionospheric tomography algorithms can be divided into two classes: pixel based methods and nonpixel based methods. Since different algorithms respond to time variations in the ionosphere in different ways, this paper will present results from both a pixel based algorithm and a nonpixel based algorithm. Furthermore, since ionosonde information is often used to supplement TEC data, this paper will also present results using ionosonde information.

The pixel based algorithm that will be used to demonstrate the effects of motion in the source image is smoothness and conjugate gradients (SCG) [5]. The SCG algorithm combines smoothness constraints similar to those proposed by Fehmers [6] with solution by conjugate gradients.

It is known that ionospheric electron density tends to be constant in the horizontal direction, smooth in the vertical direction, and very small at low and high altitudes. These characteristics are incorporated into the SCG algorithm by minimizing the first derivative in the horizontal direction, the second derivative in the vertical direction, and the value of the pixels at the bottom and top of the reconstruction. This leads to a large, sparse system of equations that can be solved using any convenient least squares technique. The method of conjugate gradients will be used here, since its convergence is not affected by inconsistent data.

The nonpixel based algorithm that will be used to demonstrate the effects of motion in the source image is the residual correction method (RCM) [7]. The image $g(\theta, r)$ is expressed as the weighted sum of orthonormal basis images

$$g(\theta, r) = \sum_{k=1}^{K} x_k \phi_k(\theta, r), \quad (1)$$

where the weights $\{x_1 \cdots x_K\}$ are unknown. The set of basis images $\{\phi_1 \cdots \phi_K\}$ is separable; the Fourier basis is used in the horizontal direction, and empirical orthonormal basis functions are used in the vertical direction.

Even with empirical orthonormal functions for the vertical basis, the reconstruction is generally not uniquely determined, so the reconstruction problem is partitioned into a set of smaller problems, each of which possesses a unique solution. The RCM algorithm then iteratively cycles through the partitions of the problem. RCM does not guarantee nonnegativity of the solution, but if the data are consistent with the *a priori* information, then RCM tends to produce a nonnegative solution.

3. ARTIFACTS DUE TO MOTION

In other applications of tomography where complete projection data are available, imaging artifacts from movement of an object during data collection include smearing and streaking. Even very little motion can produce obvious artifacts in the reconstruction. Since ionospheric electron density is a smooth function, and the projection data for an IT system are incomplete, some of the artifacts produced by movement in the ionosphere during data collection are more difficult to identify than the artifacts produced in other applications of tomography. In general, significant motion in the ionosphere can produce distortions in the reconstruction that resemble valid ionospheric features.

For any TEC data set, no matter how corrupted by time variations in the ionosphere, there always exists a source image that produces the observed data. This is particularly true for IT because the projection data are incomplete. Therefore the TEC data cannot be inconsistent with itself; however, it may be inconsistent with *a priori* assumptions. For example, the reconstructed image could contain features that are clearly impossible, such as negative electron densities.

For IT the types of errors that can be caused by movement of the ionosphere during data collection can be summarized as follows: (1) clearly visible artifacts, e.g. streaking; (2) increased magnitude of residual; (3) negative pixels in reconstruction; (4) geometric distortion, e.g. features displaced from actual position. The presence of clearly visible artifacts can be used to detect images that are corrupted by motion in the source image, but these are not often visible in IT reconstructions. The magnitude of the residual and number of negative pixels can, under some conditions, be used to detect corrupted images. Geometric distortion is a serious error that cannot be used to detect corrupted images.

The effects of movement in the ionosphere during data collection will be evaluated in terms of the four categories stated above. Both SCG and RCM will be evaluated. Also, SCG with ionosonde data in addition to TEC data will be evaluated to determine the effect of additional information on the reconstruction errors.

4. SIMULATIONS

The source image used in the simulations presented in this paper is shown in Figure 1a. TEC data was simulated for this image using 13 receivers from $-30°$ to $30°$ latitude in increments of $5°$ and satellite positions from $-35°$ to $35°$ latitude in increments of $0.25°$. In the simulations where ionosonde data was used, data was simulated for 7 ionosondes from $-30°$ to $30°$ latitude in increments of $10°$.

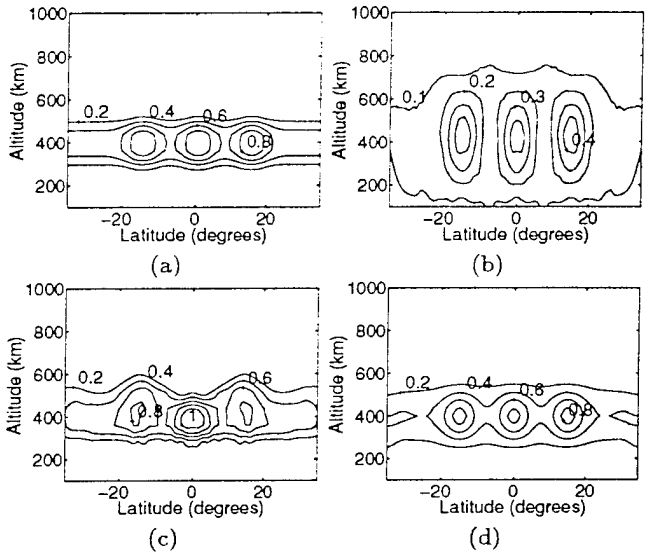

Figure 1: Original image and reconstructions using static data: (a) Original image. (b) Reconstruction using SCG. (c) Reconstruction using SCG with ionosonde information. (d) Reconstruction using RCM.

The reconstructions of Figure 1 show how each of the algorithms behave when the source image is not moving. The reconstruction in Figure 1b was performed using the SCG algorithm. The reconstruction is smeared in the vertical direction, because the SCG algorithm uses minimal *a priori* information. However, the three peaks are reconstructed at the correct latitude and altitude.

The reconstruction in Figure 1c was performed using the SCG algorithm with ionosonde information. Since an ionosonde is located directly under the central peak, there is a significant improvement in vertical resolution for the central peak though not for the outside peaks. It is interesting to note that the resolution is increased on the top side of the central peak even though the ionosonde provides information only about the bottom side. Information about the bottom side profile is sufficient, when combined with the TEC data, to increase the resolution on both the bottom side and top side.

The reconstruction in Figure 1d was performed using the RCM algorithm. The vertical resolution is much greater for the RCM algorithm, because much stronger use is made of *a priori* information. The *a priori* information consisted of a set of 98 profiles with the altitude of the peak electron density ranging from 250 km to 550 km.

All three of the reconstructions of Figure 1 are plot-

ted using 98 pixels in the horizontal direction and 25 pixels in the vertical direction. For the SCG algorithm, this means that the reconstruction was performed using 2450 basis functions, since for the SCG algorithm each pixel is a basis function. For the RCM algorithm, 3 vertical basis functions and 21 horizontal basis function where used, for a total of 63 basis images.

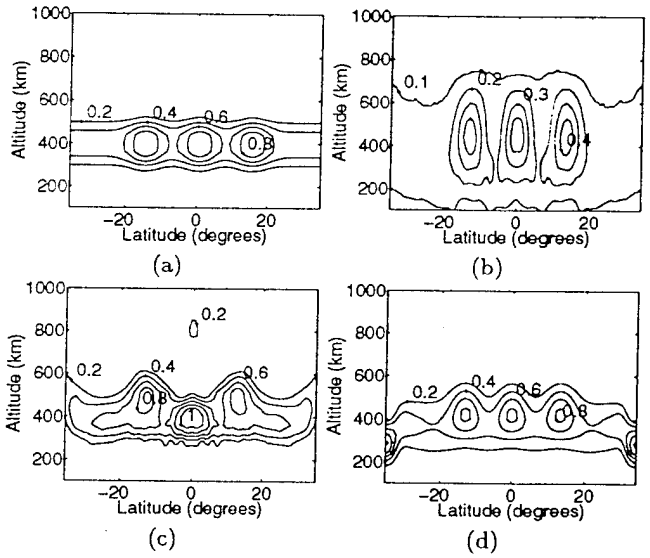

Figure 2: Original image and reconstructions where the electron density drifted to the left during data collection: (a) Original image. (b) Reconstruction using SCG. (c) Reconstruction using SCG with ionosonde information. (d) Reconstruction using RCM.

Figure 2 shows the effect of the electron density drifting to the left, in the opposite direction from the satellite motion, during data collection. The source image was allowed to drift a total of 10° from 5° right of center to 5° left of center. The source image is shown again in Figure 2a. A reconstruction using SCG with no ionosonde information is shown in Figure 2b. The outer peaks are displaced toward the center of the image, because when the outer peaks drift in the opposite direction from the satellite motion, they are located closer to the center at the time the satellite is directly overhead. All three peaks are reconstructed at a slightly higher altitude than in the source image or in the reconstruction of Figure 1b.

A reconstruction using SCG with ionosonde information is shown in Figure 2c. Clearly, motion in the ionosphere may be detected by examining how the ionosonde measurements evolve over time; however, for a static reconstruction only one set of ionosonde measurements can be included. The ionosonde measurements were taken when the satellite was at 0° latitude. The central peak is forced to the correct altitude by the data from the ionosonde located at 0°, but the outer peaks are displaced upwards even more than in Figure 2b. Also, there is an artifact at the top center of the reconstruction of Figure 2c.

A reconstruction using RCM is shown in Figure 2d. The background electron density is reconstructed at the correct altitude, but the three peaks are all displaced upwards as in Figure 2b. The distortions at the left and right edges are not significant, since there is no TEC data for those areas of the image.

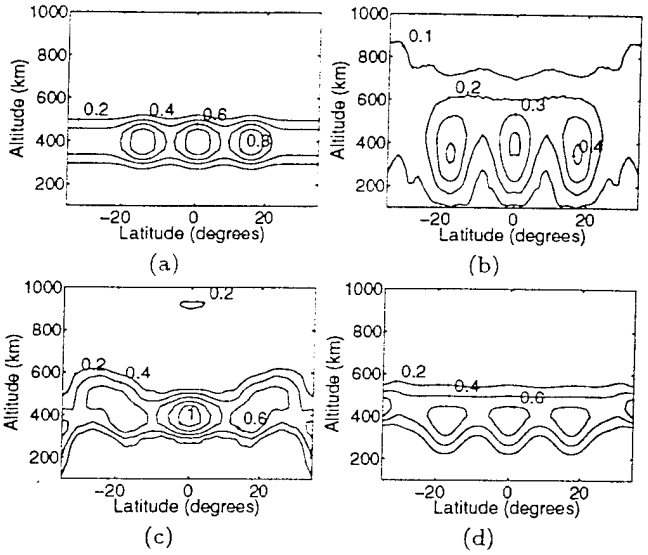

Figure 3: Original image and reconstructions where the electron density drifted to the right during data collection: (a) Original image. (b) Reconstruction using SCG. (c) Reconstruction using SCG with ionosonde information. (d) Reconstruction using RCM.

Figure 3 shows the effect of the electron density drifting to the right, in the same direction as the satellite motion, during data collection. The source image was allowed to drift a total of 10° from 5° left of center to 5° right of center. The source image is shown again in Figure 3a. A reconstruction using SCG with no ionosonde information is shown in Figure 3b. The outer peaks are displaced away from the center of the image, and all three peaks are reconstructed at a slightly higher altitude than in the source image or in the reconstruction of Figure 1b. A reconstruction using SCG with ionosonde information is shown in Figure 3c. The central peak is forced to the correct altitude by the ionosonde information, but the outer peaks are badly distorted, and there is an artifact at the top center of the image. A reconstruction using RCM is shown in Figure 3d where all three peaks are displaced downwards.

Most of the reconstructions do not show any clearly visible artifacts such as smearing or streaking. Figures 2c and 3c show very minor artifacts, probably due to the conflict between the TEC data and the ionosonde data.

Table 1 shows the magnitude of the residual vector for all 9 reconstructions as calculated for the TEC measurements only. The residual vector is the difference between the observed TEC data and TEC data calculated from the reconstruction. The SCG algorithm does not show any increase in the residual when the source image is moving. The large number of pixels and small amount of *a priori* information gives the SCG algorithm enough degrees of freedom to calculate a reconstruction to match almost any TEC data.

	Static	Mov. Left	Mov. Right
SCG	7709	7568	7219
SCG w/Iono.	2798	3831	3034
RCM	1957	6500	27191

Table 1: Length of residual vector in electrons/m^2.

When ionosonde information is included in the data for the SCG algorithm, there is a small increase in the residual when the source image is moving, but not enough to reliably determine that there is a problem. For the RCM algorithm, since it uses the strongest *a priori* information, there is a dramatic increase in the residual when the source image is moving. In order to identify reconstructions that are corrupted by movement in the ionosphere, stronger use of *a priori* information is needed.

	Static	Mov. Left	Mov. Right
SCG	12	49	0
SCG w/Iono.	956	1040	986
RCM	0	216	208

Table 2: Number of negative pixels.

Table 2 shows the number of negative pixels for all 9 reconstructions. For the SCG algorithm there is no consistent increase in the number of negative pixels when the source image is moving, and when ionosonde information is used there is only a small increase in the number of negative pixels. For the RCM algorithm there is a much larger increase in the number of negative pixels when the source image is moving. Again, stronger use of *a priori* information is needed to identify reconstructions that are corrupted by movement in the ionosphere.

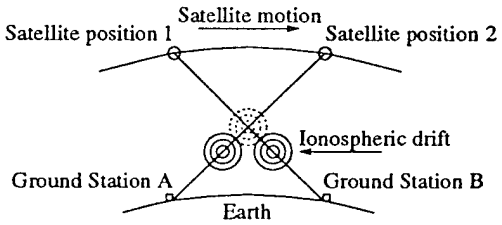

Figure 4: Diagram showing why moving ionospheric disturbances are displaced in altitude. The initial and final positions of an ionospheric disturbance are shown in solid lines, and the apparent position is shown in dotted lines.

All of the reconstructions of Figures 2 and 3 show geometric distortion of the three disturbances. The horizontal displacement of the disturbances is not actually a distortion, since the horizontal position is correct for the time when the satellite is over the region where the disturbance is found. The vertical displacement of the disturbances is a more serious problem. Figure 4 illustrates why this vertical displacement occurs. When the satellite is at position 1, the data for ground station B shows the peak of the disturbance. When the satellite has moved to position 2, the disturbance has moved so that the data for ground station A shows the peak of the disturbance. When the algorithm attempts to find a fixed position for the disturbance, it locates the disturbance at the intersection of the lines 1B and 2A. Therefore the horizontal movement of the disturbance during data collection causes a vertical displacement in the reconstruction of the disturbance.

5. CONCLUSION

Time variations in the source image are a significant contributor to the errors in static reconstructions of the ionosphere. These errors include artifacts and geometric distortion. Errors due to motion in the ionosphere during data collection are serious, since geometric distortion cannot be detected from examination of a single IT reconstruction, and artifacts are difficult to identify and not always present.

The TEC data cannot be inconsistent with itself, but it can be inconsistent with *a priori* information. Therefore, it is possible to detect that a reconstruction is distorted due to motion in the source image if the reconstruction algorithm uses sufficiently strong *a priori* information. This can be accomplished by analysis of the magnitude of the residual and the number of negative pixels. Ionosonde information can be useful in detecting motion; however, inclusion of a single set of ionosonde scans in the data set can lead to additional distortion in the reconstruction and is generally not sufficient to detect motion.

Acknowledgments. This material is based upon work supported by the Office of Naval Research under grant N00014-95-1-0850.

6. REFERENCES

[1] J. R. Austen, S. J. Franke, and C. H. Liu, "Ionospheric imaging using computerized tomography," *Radio Science*, vol. 23, pp. 299–307, May–June 1988.

[2] T. D. Raymund, J. R. Austen, S. J. Franke, C. H. Liu, J. A. Klobuchar, and J. Stalker, "Application of computerized tomography to investigation of ionospheric structures," *Radio Science*, vol. 25, pp. 771–789, Sept.–Oct. 1990.

[3] K. C. Yeh and T. D. Raymund, "Limitations of ionospheric imaging by tomography," *Radio Science*, vol. 26, pp. 1361–1380, Nov.–Dec. 1991.

[4] H. Na and E. Sutton, "Resolution analysis of ionospheric tomography systems," *Int. J. Imag. Systems Technol.*, vol. 5, no. 2, pp. 169–173, 1994.

[5] E. Sutton and H. Na, "Ionospheric tomography using smoothness and conjugate gradients," Iowa Technical Report No. HN9613, University of Iowa, Iowa City, Iowa 52242, May 1996.

[6] G. C. Fehmers, "A new algorithm for ionospheric tomography," *Proceedings of the International Beacon Satellite Symposium*, pp. 52–55, July 1994.

[7] E. Sutton and H. Na, "A block iterative algorithm for tomographic reconstruction of ionospheric electron density," *Int. J. Imag. Systems Technol.*, 1996. (in press).